Rapid Communications

Intervalley polaron in atomically thin transition metal dichalcogenides

M. M. Glazov and M. A. Semina
Ioffe Institute, 194021 St. Petersburg, Russia

C. Robert, B. Urbaszek, T. Amand, and X. Marie
Université de Toulouse, INSA-CNRS-UPS, LPCNO, 135 Av. Rangueil, 31077 Toulouse, France

(Received 13 April 2019; published 8 July 2019)

We study theoretically intervalley coupling in transition metal dichalcogenide monolayers due to electron interaction with short-wavelength phonons. We demonstrate that this intervalley polaron coupling results in (i) a renormalization of the conduction band spin splitting and (ii) an increase of the electron effective masses. We also calculate the renormalization of the cyclotron energy and the Landau level splitting in the presence of an external magnetic field. An intervalley magnetophonon resonance is uncovered. Similar, but much weaker effects are also expected for the valence band holes. These results might help to resolve the discrepancy between *ab initio* values of the electron effective masses and the ones deduced from magnetotransport measurements.

DOI: 10.1103/PhysRevB.100.041301

Introduction. Fascinating electronic and optical properties of two-dimensional (2D) materials like graphene, transition metal dichalcogenide (TMD) monolayers (MLs), atomically thin hexagonal boron nitride, black phosphorous, and others have attracted strong interest [1–3]. The unusual band structure of TMD MLs with two valleys in conduction and valence bands, where the spin degeneracy of the electron and hole states is removed and the spin and valley degrees of freedom are locked [4,5] has made 2D TMD crystals extremely attractive for the study of spintronic and valleytronic effects [6–9]. Chiral selection rules combined with strong excitonic effects provide unprecedented access to spin and valley indices of charge carriers by optical means [10,11]. For in-depth studies of TMD MLs and the development of possible applications, the basic band structure parameters, including band gap and effective masses, should be reliably established both from experiments and modeling.

Optical spectroscopy has made it possible to determine key parameters such as exciton band gap, binding energy, and Landé factor and to evaluate the reduced masses of the electron-hole pairs from high magnetic field experiments [10,12]. The single electron parameters, namely, the effective masses of charge carriers and their individual g factors are usually hard to determine optically. These quantities are, as a rule, inferred from transport measurements. Thanks to the improvement of carrier mobility obtained in hBN encapsulated TMD monolayers [13,14], quantum transport measurements have been recently performed.

Observation of Landau levels has allowed one to determine the effective masses of the charge carriers in the valence and conduction bands [14–18]. Interestingly, while the measured valence band (VB) hole masses are in good agreement with both first-principles modeling and angle-resolved photoemission spectroscopy (ARPES) measurements [19,20], the discrepancies for the conduction band (CB) effective masses in Mo-based monolayers are substantial [16,17] and can hardly be related to electron-electron interaction and inaccuracies in density functional theory (DFT) calculations. The transport measurements in both MoS_2 and $MoSe_2$ MLs yield a characteristic CB electron effective mass of 0.7–0.8m_0, typically twice larger than those deduced from DFT calculations (m_0 is the free electron mass) [21,22].

Here we demonstrate a pathway which could improve the agreement between the theory and the experiment for conduction band masses in TMD MLs. We show that two valleys $\boldsymbol{K}$ and $\boldsymbol{K}'$ can be coupled by the phonons with wave vectors close to the edge of the Brillouin zone (BZ). Let us recall that the spin-up and the spin-down CB bands in each nonequivalent valley $\boldsymbol{K}$ and $\boldsymbol{K}'$ are split by the spin-orbit (SO) interaction, with a typical energy difference, Δ_{cb}, of a few tens of meV (see Fig. 1) [21,23]. The intervalley electron-phonon coupling is stronger for the CB because electron-phonon interaction is largely spin conserving, thus strong SO splitting of the VB (of the order of hundreds of meV) suppresses the mixing. We develop an analytical model for the suggested type of polaron and demonstrate that the intervalley polaron effect results in the renormalization of both the CB spin splitting and the effective masses of the electrons. We discuss also the renormalization of the Landau level energies due to the intervalley polaron effect. Our simple model indicates an increase of the electron effective mass due to an intervalley polaron, in qualitative agreement with transport measurements, but the quantitative agreement with the experiments requires an exaggerated coupling constant possibly due to oversimplification of the model.

Intervalley electron-phonon interaction. Electrons propagating through the crystal interact with the host lattice atoms and produce local deformations of the lattice. Thus, the periodic potential experienced by the electron is modified resulting in a modification of the electron energy, and the dragging of the crystal lattice deformation with the electron gives rise to an increase of electrons effective mass as a result of the polaron effect [24–28]. This effect was found to be important to explain effective mass variations in many different

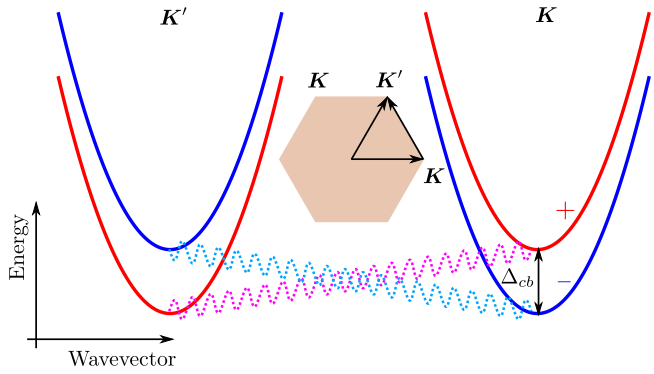

FIG. 1. Schematic illustration of the conduction subbands in the vicinity of the $\boldsymbol{K}$ and $\boldsymbol{K}'$ points at the BZ edge. Inset shows the hexagonal BZ. Wiggly lines illustrate phonon-induced coupling between the valleys. Signs "+" and "−" denote top and bottom subbands.

semiconductors [29–32]. Quantum mechanically, electron-phonon interaction due to virtual processes of emission and reabsorption of the phonon by the electron gives rise to the formation of the phonon cloud surrounding the electron and renormalizes its dispersion. In the second-order perturbation theory the electron self-energy, $\Sigma_{\boldsymbol{p}}(\varepsilon)$, due to the coupling with phonons can be written at zero temperature as

$$\Sigma_{\boldsymbol{p}}(\varepsilon) = \sum_{\boldsymbol{q},\alpha;j} \frac{\left|M^{j}_{\boldsymbol{q},\alpha}\right|^2}{\varepsilon - \hbar\Omega_{\boldsymbol{q},\alpha} - E^{j}_{\boldsymbol{p}-\boldsymbol{q}} + i\delta}. \tag{1}$$

Here $\boldsymbol{p}$ is the electron wave vector in the crystal, ε is the energy variable, $\boldsymbol{q}$ is the phonon wave vector, α enumerates the phonon branches, j enumerates the intermediate states of the electron, $M^{j}_{\boldsymbol{q},\alpha}$ is the electron-phonon coupling matrix element, $\Omega_{\boldsymbol{q},\alpha}$ is the frequency of the corresponding phonon mode, and $E^{j}_{\boldsymbol{p}}$ is the electron dispersion in the state j; the term with $\delta \to +0$ in the denominator ensures the causality. The self-energy (1) describes the electron energy and dispersion renormalization in the second order in the electron-phonon interaction.

Leading contributions to Eq. (1) are provided mainly by the nearest intermediate states and also by high-symmetry points of the BZ where the phonon dispersion is flat and the density of states is increased [33]. Analysis of the TMD MLs CB structure shows that the main contributions to the self-energy are produced by the intermediate states in the same band and the same valley, i.e., by the standard, *intravalley*, Fröhlich-like polaron, studied, e.g., in Refs. [34–36] as well as by the intermediate states in the opposite valley ($\boldsymbol{K}'$ for the electrons in the $\boldsymbol{K}$ valley and vice versa), which result in the *intervalley* polaron, not investigated so far. A key difference for the intervalley polaron compared with the intravalley polaron is the presence of the CB spin splitting in the energy denominator.

The results on the intravalley polaron are summarized in the Supplemental Material (SM), which also contains justification of the applicability of the second-order perturbation theory to calculate $\Sigma_{\boldsymbol{p}}(\varepsilon)$ in Eq. (1) for the TMD ML system [37]. Here we focus on the intervalley polaron which results in the coupling of electron states in the $\boldsymbol{K}$ and $\boldsymbol{K}'$ valleys as schematically shown in Fig. 1. Generally, in order to calculate the self energy, the electron and phonon dispersions across the whole BZ are needed; here we take into account the contribution coming from the vicinity of $\boldsymbol{K}'$ (for the $\boldsymbol{K}$ valley electron) where the density of states is the largest. We focus on the renormalization of electron states in the $\boldsymbol{K}$ valley; correspondingly, we replace $M^{i}_{\boldsymbol{q},\alpha}$ by $M^{i}_{\boldsymbol{K},\alpha}$, its value for $\boldsymbol{q} = \boldsymbol{K}$, and we also disregard the phonon dispersion replacing $\hbar\Omega_{\boldsymbol{q},\alpha}$ by $\hbar\Omega_{\boldsymbol{K},\alpha}$. In what follows we omit the subscript α (keeping in mind that in the final result one has to sum over all appropriate phonon modes) and take into account that the spin is conserved by the electron-phonon interaction. Changing the integration variable from $\boldsymbol{q}$ to $\boldsymbol{q}' = \boldsymbol{q} - \boldsymbol{K}$, and taking into account that for the electron in the top (bottom) spin subband the intermediate state energy reads $E^{j}_{\boldsymbol{p}-\boldsymbol{q}} \approx \mp\Delta_{cb} + E_{\boldsymbol{p}-\boldsymbol{q}'}$, $E_{\boldsymbol{p}} = \hbar^2 p^2/(2m)$, with m being the bare CB effective mass [50], we arrive at

$$\Sigma_{\boldsymbol{p},\pm}(\varepsilon) = -\frac{\beta_{\boldsymbol{K}}(\Delta_{cb} + \hbar\Omega_{\boldsymbol{K}})}{4\pi} \times \int_0^{E_Q} \frac{dE}{\sqrt{(\varepsilon - E_{\boldsymbol{p}} \pm \Delta_{cb} - \hbar\Omega_{\boldsymbol{K}} - E)^2 - 4E_{\boldsymbol{p}}E}}. \tag{2}$$

Here subscripts correspond to the top (+) and bottom (−) spin subbands, $\Delta_{cb} > 0$. The effective dimensionless intervalley coupling constant in Eq. (2) reads

$$\beta_{\boldsymbol{K}} = \frac{2\mathcal{S}m|M_{\boldsymbol{K}}|^2}{\hbar^2(\Delta_{cb} + \hbar\Omega_{\boldsymbol{K}})}, \tag{3}$$

and the cut-off energy $E_Q = \hbar^2 Q^2/2m$ with the cut-off wave vector $Q \sim |\boldsymbol{K}|$ needed to avoid the logarithmic divergence of the integral; $\mathcal{S}$ is the normalization area. We have omitted the infinitesimal term $i\delta$ in the denominator for brevity. It is worth stressing that $\beta_{\boldsymbol{K}}$ depends not only on the matrix element of the electron-phonon intervalley interaction but also on the combination of the CB spin splitting and the phonon energy $\Delta_{cb} + \hbar\Omega_{\boldsymbol{K}}$. The logarithmic divergence does not mean particularly strong electron-phonon coupling; it demonstrates the limitations of the analytical approach with parabolic bands, flat dispersion of phonons, and momentum-independent coupling.

Renormalization of band parameters. The electron-phonon interaction produces a noticeable effect on conduction subband energies [51]. We predict a significant renormalization effect of the CB spin splitting. Indeed, as is seen from Fig. 1, for the electron in the lower spin subband the intermediate state has a higher energy, $\Delta_{cb} + \hbar\Omega_{\boldsymbol{K}}$, while for the electron in the higher spin subband the intermediate state has a lower energy, $-\Delta_{cb} + \hbar\Omega_{\boldsymbol{K}}$. Under the condition $\hbar\Omega_{\boldsymbol{K}} > \Delta_{cb}$ both subbands are pushed by the electron-phonon interaction toward the lower energies, but the shift of the upper subband is larger (see inset in Fig. 2). The variation of the CB spin splitting can be recast as

$$\delta\Delta_{cb} = \lim_{p\to 0}[\Sigma_{\boldsymbol{p},+}(E_{\boldsymbol{p}}) - \Sigma_{\boldsymbol{p},-}(E_{\boldsymbol{p}})]. \tag{4}$$

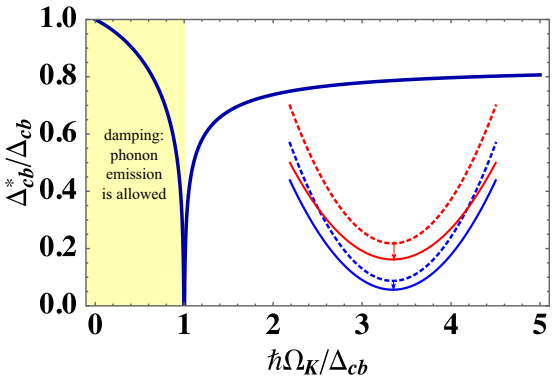

FIG. 2. Renormalized conduction band spin splitting as a function of the ratio between the phonon energy $\hbar\Omega_K$ and bare conduction band spin splitting Δ_{cb} calculated for $\beta_K = 1$ after Eq. (5). Filled area corresponds to the situation where $\hbar\Omega_K < \Delta_{cb}$ and the real phonon emission processes are possible. Inset demonstrates relative shifts of upper and lower spin subbands in one valley due to the electron-phonon interaction with another valley and the renormalization of the effective mass (exaggerated for illustration).

We introduce the renormalized CB spin splitting $\Delta^*_{cb} = \Delta_{cb} + \mathrm{Re}\{\delta\Delta_{cb}\}$ and present it in the form

$$\Delta^*_{cb} = \Delta_{cb}\left[1 - \frac{\beta_K}{4\pi}\left(1 + \frac{\hbar\Omega_K}{\Delta_{cb}}\right)\ln\left(\frac{\hbar\Omega_K + \Delta_{cb}}{\hbar\Omega_K - \Delta_{cb}}\right)\right]. \quad (5)$$

Note that logarithmic divergencies in the self-energies cancel and the result (5) does not depend on the cut-off energy. For $\Delta_{cb} > \hbar\Omega_K$ the argument of the logarithm becomes negative and, formally, Δ^*_{cb} acquires an imaginary part. In this case, the energy shift is given by the real part of the same expression (5). However, the intervalley transitions from the upper to the lower subband accompanied by the phonon emission become possible. The associated damping of the electron in the upper spin subband is determined by the imaginary part of Δ^*_{cb}. The calculated renormalization of the CB spin splitting is plotted in Fig. 2 as a function of the ratio $\hbar\Omega_K/\Delta_{cb}$. The singularity in the Δ^*_{cb} at $\hbar\Omega_K = \Delta_{cb}$, i.e., at the threshold of the phonon emission, results from the resonance condition where the energy of the electron in the top subband minus phonon energy equals the energy of the electron in the bottom subband. The detailed analysis of this singular behavior can be carried out by the methods developed in Ref. [52]; it is beyond the scope of the present work.

Similarly, one can extract the p^2 contribution in the self-energy and obtain the renormalization of the effective mass resulting from the intervalley polaron. We obtain for the top (+) and bottom (−) spin subbands

$$m^*_\pm = m\left(1 + \frac{\beta_K}{4\pi}\frac{\hbar\Omega_K + \Delta_{cb}}{\hbar\Omega_K \mp \Delta_{cb}}\right). \quad (6)$$

Interestingly, the polaron effect not only increases the effective masses but also leads to a difference of the mass of the two spin subbands: $m^*_+ \neq m^*_-$. Similarly to the renormalization of the Δ_{cb} the intervalley polaron effect on the masses is singular at $\hbar\Omega_K = \Delta_{cb}$, i.e., at the threshold of the phonon emission. Interestingly, the intervalley polaron effect makes both spin subbands heavier and the renormalization of the mass in the topmost subband is larger, $m^*_+ > m^*_-$ (inset in Fig. 2). Note that the interaction of the CBs with the VBs ($\boldsymbol{k}\cdot\boldsymbol{p}$ mixing) also yields a slight difference of masses for top and bottom CBs; this difference is controlled by the dimensionless ratio $\sim\Delta_{vb}/E_g$ where E_g is the band gap and Δ_{vb} the SO splitting of the VB [11,21]. In contrast to the intervalley polaron effect, this $\boldsymbol{k}\cdot\boldsymbol{p}$ mixing of the bands together with the SO coupling makes the topmost subband heavier in Mo-based MLs and lighter in W-based MLs due to different order of spin states [21].

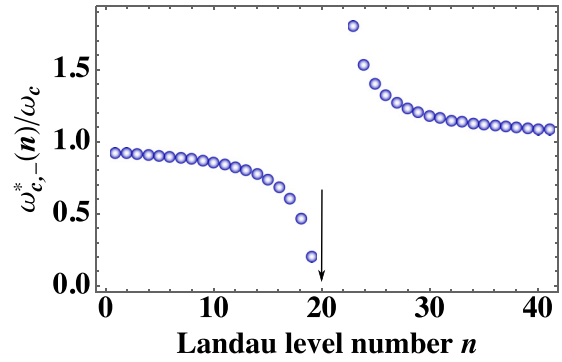

FIG. 3. Renormalized cyclotron frequency for the bottom spin subband at $\beta_K = 1$ and $\hbar\omega_c/(\hbar\Omega_K + \Delta_{cb}) = 1/20$ calculated after Eq. (9). The arrow indicates intervalley magnetophonon resonance condition, Eq. (10).

Renormalization of Landau levels. Let us now discuss the effect of the intervalley polaron on the electron spectrum in a magnetic field. We assume that the magnetic field $\boldsymbol{B}$ is applied perpendicular to the ML plane and disregard the electron Zeeman splitting assuming it to be much smaller than both the phonon energy $\hbar\Omega_K$ and the CB SO splitting Δ_{cb}. As a result, in the absence of electron-phonon interaction, the electron energy spectrum consists of the well-known series of Landau levels

$$E_n = \hbar\omega_c\left(n + \tfrac{1}{2}\right), \quad (7)$$

where $\omega_c = |eB_z/mc|$ is the electron cyclotron frequency. We calculate the correction to the energy of the nth Landau level in the second order in the intervalley electron-phonon interaction. Similarly to Eqs. (1) and (2) we obtain (cf. Ref. [35] where intravalley Fröhlich magnetopolaron in TMD ML was studied)

$$\delta E_{n,\pm} = \sum_{\boldsymbol{q}',n'k'_y} \frac{|M_K|^2|\langle n'k'_y|e^{i\boldsymbol{q}'\boldsymbol{r}}|nk_y\rangle|^2}{\hbar\omega_c(n-n') - \hbar\Omega_K \pm \Delta_{cb}}. \quad (8)$$

Here we disregarded the wave-vector dependence of the intervalley matrix element and phonon dispersion, $\pm$ refers to the electron in the top and bottom spin subbands, $\boldsymbol{q}' = \boldsymbol{q} - \boldsymbol{K}$ with $\boldsymbol{q}$ being the phonon wave vector, $|nk_y\rangle$ is the electron state in the Landau gauge, n is the Landau level number, and k_y is the component of the electron in-plane wave vector. We obtain the renormalized electron spectrum in the form of Eq. (8) with the effective cyclotron frequency $\omega^*_{c,\pm}(n)$ which depends now on the Landau level number and on the spin subband [37]:

$$\frac{\omega^*_{c,\pm}(n)}{\omega_c} = 1 - \frac{\beta_K}{4\pi(1-\eta_\pm n)}\frac{\hbar\Omega_K + \Delta_{cb}}{\hbar\Omega_K \mp \Delta_{cb}}, \quad (9)$$

where $\eta_\pm = \hbar\omega_c/(\hbar\Omega_{\boldsymbol{K}} \mp \Delta_{cb})$ characterizes the magnetic field strength.

In the limit of weak magnetic fields and low Landau levels, where $\eta_\pm n \ll 1$, we have a series of the equidistant Landau levels in each subband with the renormalized effective mass given by Eq. (6). For $\eta_\pm n \gg 1$ one recovers unperturbed Landau levels, Eq. (8), because the phonon cloud cannot follow the electron orbiting with high enough frequency. Strong renormalization of the cyclotron frequency occurs for the top spin subband at $\hbar\Omega_{\boldsymbol{K}} = \Delta_{cb}$ where the resonant emission of phonons becomes possible. Another strong feature in $\omega^*_{c,\pm}(n)$ occurs at

$$n = \left\lfloor \frac{1}{\eta_\pm} \right\rfloor, \tag{10}$$

where $\lfloor \ldots \rfloor$ stands for the integer part (see Fig. 3). Under this condition there is an intervalley magnetphonon resonance (cf. Refs. [53,54]): The energy of the nth Landau level in one of the subbands is at resonance with the bottom of another subband in the opposite valley. In this case the polaron effect is particularly strong (arrow in Fig. 3).

Discussion. Intervalley polaron coupling in TMD MLs can be enabled by the phonons with large wave vectors $|\boldsymbol{q}| \approx |\boldsymbol{K}|$ [6,55–57]. The symmetry of relevant phonon modes is discussed in the SM [37]; for conduction band the main contribution comes from the chiral phonon mode [6,58,59] whose angular momentum component equals to ± 1 for $\boldsymbol{K}' \rightleftharpoons \boldsymbol{K}$ transfer [37]. The effect is related to the intervalley deformation potential induced by the lattice vibrations. Note that the Fröhlich interaction is long range and expected to provide negligible contribution to the intervalley polaron effect. The matrix element $M_{\boldsymbol{K}}$ in Eqs. (3) and (8) can be represented as

$$M_{\boldsymbol{K}} = \sqrt{\frac{\hbar}{2\rho\Omega_{\boldsymbol{K}}\mathcal{S}}} D_0, \tag{11}$$

where ρ is the two-dimensional mass density of the crystal, D_0 is the deformation potential parameter, and $\mathcal{S}$ is the normalization area. Substituting Eq. (11) into Eq. (3) we obtain a crude estimate for the coupling strength $\beta_{\boldsymbol{K}}$:

$$\beta_{\boldsymbol{K}} \sim \frac{D_0^2}{\hbar\Omega_{\boldsymbol{K}}(\hbar\Omega_{\boldsymbol{K}} + \Delta_{cb})} \frac{m}{\rho} \sim 0.1 \ldots 1, \tag{12}$$

at $\rho = 3 \times 10^{-7}$ g/cm^2, $m = 0.5m_0$, $D_0 \sim (1 \ldots 4) \times 10^8$ eV/cm [57], and $\hbar\Omega_K \sim \Delta_{cb} \sim 10$ meV. With this simplified model and the uncertainty of the parameters involved, we find that the coupling is not particularly strong. It will yield an increase of the bottom CB mass by ~10%. We emphasize that the exact values of key parameters such as the CB SO splitting and deformation potential parameters are not very well known. The CB SO splitting strongly varies for different DFT models [60]. The deformation potential can be roughly estimated as the ratio of atomic energy scale, ~10 eV, to the lattice constant (several angstrom) resulting in values consistent with Ref. [57]. Additional enhancement is expected for the CB states due to the presence of the $\boldsymbol{Q}$ (also denoted as $\boldsymbol{\Lambda}$) valley. The coupling constant $\beta_{\boldsymbol{Q}}$ of the intervalley polaron involving the $\boldsymbol{Q}$ valley has a similar order of magnitude.

This increase of the CB electron mass in TMD monolayer could qualitatively explain the recent measurements performed on high-quality n-type MoS_2 and $MoSe_2$ monolayers displaying well-resolved Shubnikov de Haas oscillations. These experiments yield CB mass of about $0.7m_0$ in MoS_2 MLs and $0.8m_0$ in $MoSe_2$ MLs [16,17]. Surprisingly the masses calculated with DFT approaches are much smaller, typically $(0.4–0.5)m_0$ for both MLs [21,22]. This can hardly be explained by the electron-electron interaction as the measured electron mass for both systems does not depend much on the doping density. Remarkably this discrepancy between experiment and DFT calculation does not occur for the VB, where both transport [15] and ARPES [19,20] measurements yield the effective mass of about $0.4m_0$, in agreement with the DFT calculations [61]. The standard Fröhlich polaron effect could not explain the increase of mass observed for CB only as it should affect in a similar manner both electrons and holes. The same argument rules out possible effects of interfacial polarons due to electron-phonon coupling at the interfaces between the TMD ML and hBN [62]. In contrast, the intervalley polaron effect, as explained above, yields an increase of the CB mass (compared to the mass calculated with DFT) but produces negligible effect on the VB mass because of much larger VB SO splitting. Estimates after Eq. (12) for the VB yields the value $\beta^{vb}_{\boldsymbol{K}} \sim (\hbar\Omega_{\boldsymbol{K}} + \Delta_{cb})/\Delta_{vb}\beta_{\boldsymbol{K}} \sim \beta_{\boldsymbol{K}}/10$. Recent magneto-optical spectroscopy of TMD MLs [63] reveals an increase of the mass m in Mo-based MLs, indicating the possible importance of the intervalley polaron effect for magnetoexcitons

Our calculations also predict a significant decrease of the CB SO splitting due to intervalley polaron effect (Fig. 2). We suggest that the polaron effect should be taken into account when comparing measured SO splitting [16,17] values to DFT.

Note, that the intervalley polaron mixes bright and momentum-forbidden excitonic states and does not affect the optical selection rules in no-phonon transitions, but polaron formation could influence the spin and valley relaxation.

Conclusion. We have developed the theory of a type of polaron corresponding to phonon-induced coupling between the two nonequivalent valleys of transition metal dichalcogenide monolayers. This intervalley polaron associated to short-wavelength phonons results in both an increase of the electron effective mass and a decrease of the conduction band spin-orbit splitting. In the presence of an external magnetic field it will also lead to the renormalization of the cyclotron energy and the Landau level splitting. In contrast the intervalley polaron has negligible effects on the valence band due to its much larger spin-orbit splitting.

Acknowledgments. We are grateful to H. Dery for very stimulating discussions. M.A.S. and M.M.G. acknowledge partial support from LIA ILNACS through the RFBR project 17-52-16020. M.M.G. was partially supported by the RFBR project 17-02-00383. M.A.S. also acknowledges partial support of the Government of the Russian Federation (Project No. 14.W03.31.0011 at the Ioffe Institute). We acknowledge funding from ANR 2D-vdW-Spin, ANR VallEx, and ANR MagicValley. X.M. also acknowledges the Institut Universitaire de France.

[1] A. K. Geim and K. S. Novoselov, The rise of graphene, Nat. Mater. **6**, 183 (2007).

[2] A. K. Geim and I. V. Grigorieva, Van der Waals heterostructures, Nature (London) **499**, 419 (2013).

[3] P. Ajayan, P. Kim, and K. Banerjee, Two-dimensional van der Waals materials, Phys. Today **69**(9), 38 (2016).

[4] D. Xiao, G.-B. Liu, W. Feng, X. Xu, and W. Yao, Coupled Spin and Valley Physics in Monolayers of MoS_2 and Other Group-VI Dichalcogenides, Phys. Rev. Lett. **108**, 196802 (2012).

[5] X. Xu, W. Yao, D. Xiao, and T. F. Heinz, Spin and pseudospins in layered transition metal dichalcogenides, Nat. Phys. **10**, 343 (2014).

[6] Y. Song and H. Dery, Transport Theory of Monolayer Transition-Metal Dichalcogenides through Symmetry, Phys. Rev. Lett. **111**, 026601 (2013).

[7] H. Dery and Y. Song, Polarization analysis of excitons in monolayer and bilayer transition-metal dichalcogenides, Phys. Rev. B **92**, 125431 (2015).

[8] G. Wang, C. Robert, M. M. Glazov, F. Cadiz, E. Courtade, T. Amand, D. Lagarde, T. Taniguchi, K. Watanabe, B. Urbaszek, and X. Marie, In-Plane Propagation of Light in Transition Metal Dichalcogenide Monolayers: Optical Selection Rules, Phys. Rev. Lett. **119**, 047401 (2017).

[9] P. Dey, L. Yang, C. Robert, G. Wang, B. Urbaszek, X. Marie, and S. A. Crooker, Gate-Controlled Spin-Valley Locking of Resident Carriers in WSe_2 Monolayers, Phys. Rev. Lett. **119**, 137401 (2017).

[10] G. Wang, A. Chernikov, M. M. Glazov, T. F. Heinz, X. Marie, T. Amand, and B. Urbaszek, Colloquium: Excitons in atomically thin transition metal dichalcogenides, Rev. Mod. Phys. **90**, 021001 (2018).

[11] M. V. Durnev and M. M. Glazov, Excitons and trions in two-dimensional semiconductors based on transition metal dichalcogenides, Phys. Usp. **61**, 825 (2018).

[12] A. V. Stier, N. P. Wilson, K. A. Velizhanin, J. Kono, X. Xu, and S. A. Crooker, Magnetooptics of Exciton Rydberg States in a Monolayer Semiconductor, Phys. Rev. Lett. **120**, 057405 (2018).

[13] F. Cadiz, E. Courtade, C. Robert, G. Wang, Y. Shen, H. Cai, T. Taniguchi, K. Watanabe, H. Carrere, D. Lagarde *et al.*, Excitonic Linewidth Approaching the Homogeneous Limit in MoS_2-Based van der Waals Heterostructures, Phys. Rev. X **7**, 021026 (2017).

[14] M. V. Gustafsson, M. Yankowitz, C. Forsythe, D. Rhodes, K. Watanabe, T. Taniguchi, J. Hone, X. Zhu, and C. R. Dean, Ambipolar Landau levels and strong band-selective carrier interactions in monolayer WSe_2, Nat. Mater. **17**, 411 (2018).

[15] B. Fallahazad, H. C. P. Movva, K. Kim, S. Larentis, T. Taniguchi, K. Watanabe, S. K. Banerjee, and E. Tutuc, Shubnikov–De Haas Oscillations of High-Mobility Holes in Monolayer and Bilayer WSe_2: Landau Level Degeneracy, Effective Mass, and Negative Compressibility, Phys. Rev. Lett. **116**, 086601 (2016).

[16] S. Larentis, H. C. P. Movva, B. Fallahazad, K. Kim, A. Behroozi, T. Taniguchi, K. Watanabe, S. K. Banerjee, and E. Tutuc, Large effective mass and interaction-enhanced Zeeman splitting of K-valley electrons in $MoSe_2$, Phys. Rev. B **97**, 201407(R) (2018).

[17] R. Pisoni, A. Kormányos, M. Brooks, Z. Lei, P. Back, M. Eich, H. Overweg, Y. Lee, P. Rickhaus, K. Watanabe, T. Taniguchi, A. Imamoglu, G. Burkard, T. Ihn, and K. Ensslin, Interactions and Magnetotransport through Spin-Valley Coupled Landau Levels in Monolayer MoS_2, Phys. Rev. Lett. **121**, 247701 (2018).

[18] J. Lin, T. Han, B. A. Piot, Z. Wu, S. Xu, G. Long, L. An, P. Cheung, P.-P. Zheng, P. Plochocka, X. Dai, D. K. Maude, F. Zhang, and N. Wang, Determining interaction enhanced valley susceptibility in spin-valley-locked MoS_2, Nano Lett. **19**, 1736 (2019).

[19] Y. Zhang, T.-R. Chang, B. Zhou, Y.-T. Cui, H. Yan, Z. Liu, F. Schmitt, J. Lee, R. Moore, Y. Chen, H. Lin, H.-T. Jeng, S.-K. Mo, Z. Hussain, A. Bansil, and Z.-X. Shen, Direct observation of the transition from indirect to direct bandgap in atomically thin epitaxial $MoSe_2$, Nat. Nanotechnol. **9**, 111 (2013).

[20] W. Jin, P.-C. Yeh, N. Zaki, D. Zhang, J. T. Sadowski, A. Al-Mahboob, A. M. van der Zande, D. A. Chenet, J. I. Dadap, I. P. Herman, P. Sutter, J. Hone, and R. M. Osgood, Direct Measurement of the Thickness-Dependent Electronic Band Structure of MoS_2 Using Angle-Resolved Photoemission Spectroscopy, Phys. Rev. Lett. **111**, 106801 (2013).

[21] A. Kormanyos, G. Burkard, M. Gmitra, J. Fabian, V. Zólyomi, N. D. Drummond, and V. Fal'ko, $\boldsymbol{k}\cdot\boldsymbol{p}$ theory for two-dimensional transition metal dichalcogenide semiconductors, 2D Mater. **2**, 022001 (2015).

[22] D. Wickramaratne, F. Zahid, and R. K. Lake, Electronic and thermoelectric properties of few-layer transition metal dichalcogenides, J. Chem. Phys. **140**, 124710 (2014).

[23] K. Kośmider, J. W. González, and J. Fernández-Rossier, Large spin splitting in the conduction band of transition metal dichalcogenide monolayers, Phys. Rev. B **88**, 245436 (2013).

[24] L. D. Landau, Über die bewegung der elektronen in kristallgitter, Phys. Z. Sowjetunion **3**, 644 (1933).

[25] S. I. Pekar, Local quantum states of electrons in an ideal ion crystal, Zh. Eksp. Teor. Fiz. **16**, 341 (1946).

[26] L. D. Landau and S. I. Pekar, Effective mass of a polaron, Zh. Eksp. Teor. Fiz. **18**, 419 (1948).

[27] H. Fröhlich, Electrons in lattice fields, Adv. Phys. **3**, 325 (1954).

[28] A. S. Alexandrov and J. T. Devreese, *Advances in Polaron Physics* (Springer, Berlin/Heidelberg, 2010).

[29] M. Grynberg, S. Huant, G. Martinez, J. Kossut, T. Wojtowicz, G. Karczewski, J. M. Shi, F. M. Peeters, and J. T. Devreese, Magnetopolaron effect on shallow indium donors in CdTe, Phys. Rev. B **54**, 1467 (1996).

[30] G. Ploner, J. Smoliner, G. Strasser, M. Hauser, and E. Gornik, Energy levels of quantum wires determined from magnetophonon resonance experiments, Phys. Rev. B **57**, 3966 (1998).

[31] T. Itoh, M. Nishijima, A. I. Ekimov, C. Gourdon, A. L. Efros, and M. Rosen, Polaron and Exciton-Phonon Complexes in CuCl Nanocrystals, Phys. Rev. Lett. **74**, 1645 (1995).

[32] J. L. M. van Mechelen, D. van der Marel, C. Grimaldi, A. B. Kuzmenko, N. P. Armitage, N. Reyren, H. Hagemann, and I. I. Mazin, Electron-Phonon Interaction and Charge Carrier Mass Enhancement in $SrTiO_3$, Phys. Rev. Lett. **100**, 226403 (2008).

[33] D. Christiansen, M. Selig, G. Berghäuser, R. Schmidt, I. Niehues, R. Schneider, A. Arora, S. M. de Vasconcellos, R. Bratschitsch, E. Malic *et al.*, Phonon Sidebands in Monolayer Transition Metal Dichalcogenides, Phys. Rev. Lett. **119**, 187402 (2017).

[34] P.-F. Li and Z.-W. Wang, Optical absorption of Fröhlich polaron in monolayer transition metal dichalcogenides, J. Appl. Phys. **123**, 204308 (2018).

[35] Q. Chen, W. Wang, and F. M. Peeters, Magneto-polarons in monolayer transition-metal dichalcogenides, J. Appl. Phys. **123**, 214303 (2018).

[36] D. Van Tuan, B. Scharf, I. Žutić, and H. Dery, Intervalley plasmons in crystals, arXiv:1901.02567.

[37] See Supplemental Material at http://link.aps.org/supplemental/10.1103/PhysRevB.100.041301 for discussion of the applicability of the model, details of derivation, relation to the Holstein polaron and the symmetry analysis of the involved phonons, which includes Refs. [38–49].

[38] T. Sohier, M. Calandra, and F. Mauri, Two-dimensional Fröhlich interaction in transition-metal dichalcogenide monolayers: Theoretical modeling and first-principles calculations, Phys. Rev. B **94**, 085415 (2016).

[39] M. Danovich, I. L. Aleiner, N. D. Drummond, and V. I. Fal'ko, Fast relaxation of photo-excited carriers in 2-D transition metal dichalcogenides, IEEE J. Sel. Top. Quantum Electron. **23**, 1 (2017).

[40] M. A. Smondyrev, Diagrams in the polaron model, Theor. Math. Phys. **68**, 653 (1986).

[41] Y. Xiao, Z.-Q. Li, and Z.-W. Wang, Polaron effect on the bandgap modulation in monolayer transition metal dichalcogenides, J. Phys.: Condens. Matter **29**, 485001 (2017).

[42] R. P. Feynman, Slow electrons in a polar crystal, Phys. Rev. **97**, 660 (1955).

[43] M. Matsuura, Discontinuity of the surface polaron, Solid State Commun. **44**, 1471 (1982).

[44] W. J. Huybrechts, Ground-state energy and effective mass of a polaron in a two-dimensional surface layer, Solid State Commun. **28**, 95 (1978).

[45] W. Xiaoguang, F. M. Peeters, and J. T. Devreese, Exact and approximate results for the ground-state energy of a Fröhlich polaron in two dimensions, Phys. Rev. B **31**, 3420 (1985).

[46] T. Holstein, Studies of polaron motion: Part I. The molecular-crystal model, Ann. Phys. (NY) **8**, 325 (1959).

[47] M. Kang, S. W. Jung, W. J. Shin, Y. Sohn, S. H. Ryu, T. K. Kim, M. Hoesch, and K. S. Kim, Holstein polaron in a valley-degenerate two-dimensional semiconductor, Nat. Mater. **17**, 676 (2018).

[48] J. Ribeiro-Soares, R. M. Almeida, E. B. Barros, P. T. Araujo, M. S. Dresselhaus, L. G. Cançado, and A. Jorio, Group theory analysis of phonons in two-dimensional transition metal dichalcogenides, Phys. Rev. B **90**, 115438 (2014).

[49] B. R. Carvalho, Y. Wang, S. Mignuzzi, D. Roy, M. Terrones, C. Fantini, V. H. Crespi, L. M. Malard, and M. A. Pimenta, Intervalley scattering by acoustic phonons in two-dimensional MoS_2 revealed by double-resonance Raman spectroscopy, Nat. Commun. **8**, 14670 (2017).

[50] We neglect the difference of the electron effective masses in the two spin subbands due to spin-orbit coupling and $\boldsymbol{k}\cdot\boldsymbol{p}$ mixing.

[51] For the sake of simplicity, the overall shift of the conduction band $\propto \beta_{\boldsymbol{K}} \ln(E_Q/\Delta_{cb})$ is disregarded.

[52] I. B. Levinson and É. I. Rashba, Bound states of electrons and excitons with optical phonons in semiconductors, Sov. Phys. Usp. **15**, 663 (1973).

[53] V. L. Gurevich and Y. A. Firsov, A new oscillation mode of the longitudinal magnetoresistance of semiconductors, J. Exp. Theor. Phys. **20**, 489 (1965).

[54] Y. A. Firsov, V. L. Gurevich, R. V. Parfeniev, and S. S. Shalyt, Investigation of a New Type of Oscillations in the Magnetoresistance, Phys. Rev. Lett. **12**, 660 (1964).

[55] A. Molina-Sánchez and L. Wirtz, Phonons in single-layer and few-layer MoS_2 and WS_2, Phys. Rev. B **84**, 155413 (2011).

[56] K. Kaasbjerg, K. S. Thygesen, and K. W. Jacobsen, Phonon-limited mobility in n-type single-layer MoS_2 from first principles, Phys. Rev. B **85**, 115317 (2012).

[57] Z. Jin, X. Li, J. T. Mullen, and K. W. Kim, Intrinsic transport properties of electrons and holes in monolayer transition-metal dichalcogenides, Phys. Rev. B **90**, 045422 (2014).

[58] L. Zhang and Q. Niu, Chiral Phonons at High-Symmetry Points in Monolayer Hexagonal Lattices, Phys. Rev. Lett. **115**, 115502 (2015).

[59] H. Zhu, J. Yi, M.-Y. Li, J. Xiao, L. Zhang, C.-W. Yang, R. A. Kaindl, L.-J. Li, Y. Wang, and X. Zhang, Observation of chiral phonons, Science **359**, 579 (2018).

[60] J. P. Echeverry, B. Urbaszek, T. Amand, X. Marie, and I. C. Gerber, Splitting between bright and dark excitons in transition metal dichalcogenide monolayers, Phys. Rev. B **93**, 121107(R) (2016).

[61] The carrier densities in the transport measurements for holes are similar to the measurements for electrons discussed above.

[62] C. Chen, J. Avila, S. Wang, Y. Wang, M. Mucha-Kruczyński, C. Shen, R. Yang, B. Nosarzewski, T. P. Devereaux, G. Zhang *et al.*, Emergence of interfacial polarons from electron–phonon coupling in graphene/h-BN van der Waals heterostructures, Nano Lett. **18**, 1082 (2018).

[63] M. Goryca, J. Li, A. V. Stier, S. A. Crooker, T. Taniguchi, K. Watanabe, E. Courtade, S. Shree, C. Robert, B. Urbaszek, and X. Marie, Revealing exciton masses and dielectric properties of monolayer semiconductors with high magnetic fields, arXiv:1904.03238.